

# HYBRID INTEGRATED TUNABLE OPTICAL TRANSMITTER SUBSYSTEM ON A CHIP



## ABSTRACT

The need for tunable optical transmitters in optical networking is growing at a rapid rate. A tunable optical transmitter is the combination of a tunable laser, an isolator, and a modulator. Although today lasers and modulators could be integrated together on a single chip, an integrated component of this type would not be useful because the absence of an isolator between the two elements would cause optical reflections to reach the laser, leading to a high level of frequency chirp and relaxation oscillations. Therefore discrete external modulators are used, and lasers are coupled to them through discrete optical isolators. We report on recent developments in integrated active, thermo-optic, magneto-optic and electro-optic technologies that enable the production of a fully integrated tunable transmitter. This transmitter consists of a planar polymer waveguide circuit that is built on a silicon chip and in which films of a variety of materials are embedded. This subsystem on a chip includes a laser chip coupled to a thermo-optically tunable planar polymeric filter resulting in a tunable external cavity laser; an integrated magneto-optic isolator consisting of a planar polymer waveguide with inserted thin films of yttrium iron garnet for Faraday rotation, crystal ion sliced LiNbO<sub>3</sub> for half-wave retardation, and polarizers; and an electro-optic modulator consisting of a crystal ion sliced LiNbO<sub>3</sub> thin film patterned with a Mach-Zehnder interferometer and grafted into the polymer circuit, capable of operating with less than 5 Volts at modulation speeds up to 40 GHz.

**Keywords:** optoelectronics, hybrid integration, transmitter, laser, tunable filter, isolator, modulator, thermo-optics, magneto-optics, electro-optics

## INTRODUCTION

The great potential of optical integration has been recognized for decades, with the most notable advantages being size reduction, reduction in cost, performance improvement (lower loss due to fewer interfaces, reduction in transient errors when all interconnects are printed, etc.), increase in yields (due to the increase in uniformity and repeatability), increase in production volumes, reduction in need for manual labor, and faster time to market. Turning this promise into a commercial reality relies on having a versatile integration platform where any element can be integrated while achieving performance levels that are superior to those obtained in discrete components. Polymer-based planar lightwave circuits (PLCs) have advantages over their silica-based counterparts in terms of cost and flexibility in fabrication. Hybrid integrated devices on a polymer waveguide platform can have a significant impact on the future development of multifunctional on-chip devices. The polymer optical bench we have developed allows the integration of films of any material, permitting the integration of all optical building blocks in the best-performing material for each function, resulting in a hybrid subsystem on a chip with uncompromised performance and all the advantages of integration. We describe in this manuscript a hybrid integrated tunable optical transmitter realized with a laser chip, a tunable filter, an isolator, and a modulator, all integrated on one chip.

## 2. INTEGRATED TUNABLE TRANSMITTERS

An all-inclusive tunable optical transmitter integrated on a single chip is proposed. It consists of an active element (laser chip), a thermo-optic element (tunable filter that enables tuning of the laser through a tunable external cavity), a magneto-optic element (optical isolator), and an electro-optic element (modulator). The entire circuit is built into a planar polymer waveguide circuit printed on silicon. The choice of each material is made based solely on performance characteristics, since the grafting of any material is possible in this polymer optical bench. A block-diagram schematic of the integrated circuit is shown in Fig. 1.

\*louay.eldada@usa.dupont.com; phone 978.203.1300; fax 978.988.1040; <http://www.photonics.dupont.com>; 100 Fordham Road, Wilmington, MA, USA 01887

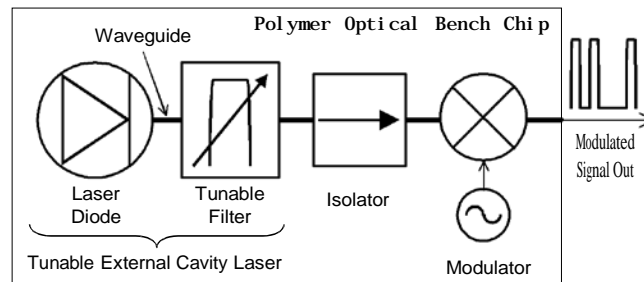


**Fig. 1.** Block diagram of the hybrid integrated tunable optical transmitter subsystem on a chip.

### 2.1. Integrated Tunable Lasers

In its essential form the laser is an optical oscillator comprising a resonant optical amplifier whose optical output is fed back to itself with matching phase. The construction of a specific laser is therefore a choice of gain medium (optical amplifier) and feedback mechanisms (a reflective surface). For most lasers two reflective elements, i.e. mirrors, are required to form an optical cavity in which the laser light oscillates. The laser diode (or semiconductor laser) in its simplest form comprises a semiconductor amplifier (gain medium) constructed from such materials as AlGaAs or InGaAsP where the gain layer is sandwiched by p-n doped GaAs or InP respectively. The heterostructure construction serves to both confine the injected carriers as well as to waveguide the light along the material interfaces. A simple cleaving of the semiconductor material results in two smooth reflecting surfaces at the semiconductor-air interface thereby completing the laser cavity. This type of laser is called the Fabry-Perot (FP) laser.

In order to make a tunable laser, a tunable wavelength selective element (filter) must be included in the laser cavity. The filter serves to reflect a narrow bandwidth of the light emitted spontaneously by the gain medium. This has the effect of allowing only light within a narrow bandwidth to oscillate, that is to lase, within the laser cavity. In the realm of tunable semiconductor lasers, a variety of tunable filter elements have been implemented. The filter elements are usually spatially periodic in structure and may either be formed from the same material as the gain material or included outside the semiconducting material as a Bragg grating fiber (Fiber Grating Laser). In both of these cases, the filter element takes the form of a periodically changing index of refraction,  $\Delta n$ , of Bragg period,  $\Lambda$ , within the waveguide.

By alternating the refractive index periodically about an average effective refractive index  $n$ , an in-line series of weakly reflecting mirrors of spacing  $\Lambda$  is created. The cumulative effect of the mirrors is to maximally reflect wavelengths  $\lambda$ , equal to  $1/N$  multiples of  $2 \cdot n \cdot \Lambda$ , where  $N \geq 1$  is an integer indicating the order of the grating period. In the case of a distributed feedback (DFB) laser, the refractive index of the gain cladding material is periodically modulated, thereby localizing both gain and Bragg grating. A small range of wavelength tunability,  $\Delta\lambda = 2$  nm, is possible in the DFB laser through thermal tuning,  $\Delta T$ , of the gain medium refractive index. The temperature increase can be assumed to be a linear function of the increased current density.<sup>1</sup> In the case of InGaAsP, where a coefficient of  $d\lambda/dT$  of  $0.1$  nm/ $^{\circ}\text{C}$  is typical, a  $\Delta T = 20$   $^{\circ}\text{C}$  is required to achieve a tuning of  $\Delta\lambda = 2$  nm. Since large ranges of laser cooling are impractical and heating reduces the lifetime of the laser as well as its power output, the DFB is not viable as widely tunable ( $\Delta\lambda > 40$  nm) laser candidate.

The DBR (Distributed Bragg Reflector), like the DFB design is a monolithic device but is arranged such that its Bragg reflectors are separate from the gain medium. Unlike the DFB where the carrier density of the gain medium saturates at lasing, the DBR reflectors are not part of the gain sections. This allows greater tuning range,  $\Delta\lambda = 5$  nm, through carrier injection tuning of the Bragg reflectors refractive index.<sup>2</sup> Nonetheless, such a limited tuning range has forced manufacturers to manufacture the in-line DBR laser, where each of three lasers covers a different 5 nm tuning range for a total tuning range of  $\Delta\lambda = 15$  nm. Since simple carrier injection or heating/cooling of the DBR is inadequate to wide wavelength tuning, a method of amplifying this limited tuning mechanisms was invented. One method is to replace the two continuously written Bragg gratings of the DBR by two sampled gratings (SG) to form a sampled grating distributed Bragg reflector (SG-DBR). The sampled gratings consist of a Bragg section of "burst" length,  $L_b$ , and a complementary uncorrugated section of length,  $L_c$ . The two sections are repeated many times to form a grating length of length,  $L$ . Since the grating is made up of a periodic structure of pattern length,  $L_p = L_c + L_b$ , the reflectivity spectrum itself will be periodic.

That is, the sampled grating will act to reflect a series of evenly spaced narrow wavelength bands of width inversely proportional to  $L$ , and of spacing inversely proportional to  $L_p$ . By designing the SG with two slightly different pattern lengths, the SG-DBR laser will function only when the reflectivity peak of one grating coincides with another peak from the other grating. Small change of one of the grating tunings leads to large tuning in the laser wavelength also known as the Vernier effect. Through the use of sampled gratings a tuning range of 30 nm was demonstrated<sup>3</sup> while continuous tuning between the 10 nm intervals was possible through simultaneous tuning of both gratings.

A number of other widely tunable laser designs have been demonstrated, the primary contender being the grating-assisted co-directional coupler with rear sampled reflector (GCSR) laser. The GCSR contains a vertical grating assisted coupler (VC) to outcouple a relatively wide wavelength range (coarse tuning) from the gain waveguide to a second waveguide. The second (passive) waveguide contains an in-line SG (fine tuning) filter which can be used to fine tune the outcoupled light. The combination of the VC and SG filters acts to reflect only a narrow wavelength band to the gain medium. Although 100 nm tuning ranges are claimed using the GCSR,<sup>4</sup> a low side mode suppression ratio (SMSR) of 25 dB makes the extreme wavelengths unusable for the ITU grid. The manufacturer, Altiton, has reduced the wide tuning range of the GCSR to cover the C-Band (1529-1561nm), thereby ensuring an adequate SMSR.

Although the SG-DBR and GCSR lasers lay claim to tuning over the C-Band, and perhaps the L-Band, their fabrication can be expensive due to the many steps required in production. Precise control of the layering and etching is inadequate which results in low yields and therefore high production costs. As an answer to this problem, the hybrid, external cavity Bragg grating laser was invented. We propose such a grating where the Bragg grating is formed in a planar polymer waveguide circuit, and is tunable thermally as described in the next section.

As in the above-described tunable lasers, the Telephotronics external cavity diode laser (ECDL) requires an optical gain medium placed between two reflectors (optical feedback elements) as well as a tunable optical filter and a phase section. The gain medium takes the form of a multi-quantum well (MQW) single-spatial-mode ridge waveguide. The waveguide is about 1 mm in length. The gain is centered at 1550 nm and has a spectral bandwidth of 60 nm and outputs 20 mW of power at room temperature. The Telephotronics ECDL uses a planar waveguide Bragg grating as its second reflecting and tunable filter element. The grating is written in a polymeric material deposited on a silicon (Si) substrate, as described in the next section on thermo-optic tunable filters. The polymeric waveguide intersects the MQW chip at a facet (inside facet) that is anti-reflection (AR) coated to  $10^{-3}$  in power reflectivity. The outside facet may be either high-reflection (HR) coated or low-reflection (LR) coated (<5%) depending upon whether the output power is to be taken from the grating or the facet, respectively. In our design, the outside facet is HR coated, allowing the output power to exit from the grating. In order to ensure continuous, mode-hop-free tuning of the ECDL, a phase section must be included in the external cavity. The purpose of the phase section is to adjust for an optimal cavity length during grating tuning. As is well known, an optical cavity or laser of optical length,  $L_0$ , will only support wavelengths,  $\lambda$ , where  $2 \cdot L_0 = m \cdot \lambda$ , and  $m$  is an integer. The result is that only cavity modes (or FP modes) of spacing  $\Delta\lambda_{FP} = \lambda^2 / (2 \cdot L_0)$  are allowed to lase within the cavity. If during the tuning of the laser by  $\Delta\lambda$ , mode hops are to be avoided, the cavity must lengthen/shorten accordingly, so that the mode number,  $m$ , remains constant. This can be summarized by the relation;  $\Delta\lambda / \Delta L_0 = \lambda / L_0$ . In the case of a 1-mm-long gain medium ( $n_{eff} = 4$ ), a grating and phase section of effective lengths  $L_{eff} = 2.9$  mm and  $L_{ps} = 5$  mm, the total optical cavity length sums to  $L_0 = 8.9$  mm. For every  $\Delta\lambda = -0.36$  nm of grating tuning (requiring a heating of the grating section by  $\Delta T_{grat} = 1$  °C), the external cavity must optically change by about  $\Delta L_0 = -2.1$   $\mu$ m. Assuming that only the grating and phase section are responsible for length tuning of the cavity, the refractive index of the phase section must be adjusted so that  $\Delta L_{ps} + \Delta L_{geff} = -2.1$   $\mu$ m. Taking into account the optical length shrinking of the grating itself (0.9  $\mu$ m), the 5-mm-long phase section offers the required optical length shortening of 1.2  $\mu$ m when heated by  $\Delta T_{ps} = 0.77$  °C. In order to heat the grating and phase section portions of the polymer waveguide, a resistive thin film metallic layer is deposited and patterned over the appropriate sections. Each heating strip is connected via two leads to two bond pads deposited and plated on the Si substrate. Sensing of the waveguide temperature is made by thermistor strips placed in the vicinity of the waveguides. Since the temperature of polymer/Si films falls off with a characteristic constant of about 20  $\mu$ m along the surface of the polymer, the thermistors must be placed within 20  $\mu$ m of the heating strips. Close proximity of the thermistors ensures an accurate measurement of the waveguide temperatures. The thermal control of the waveguide temperature, and therefore the grating peak, is achieved by connecting the thermistor and heating leads to a microcontroller. The thermal response of the waveguide heating reaches quasi

equilibrium in about 5 msec. To effect a temperature difference of  $\Delta T = 30^\circ\text{C}$  at the center of a 30- $\mu\text{m}$ -thick polymer stack, a  $\Delta T$  of 50  $^\circ\text{C}$  is required at the surface of the waveguide corresponding to about 0.25  $\text{W}/\text{mm}^2$  of heater power. The successful design of an external cavity laser depends greatly on the near elimination of facet reflectivity at the interface between the external mirror (the grating) and the MQW chip. For the case where strong feedback ( $>1\%$ ) is required to regulate the laser wavelength, a reflectivity at the laser facet/mirror interface of  $<10^{-4}$  is desirable. An AR coating value of less than  $10^{-3}$  is generally required to assure longitudinal mode stability.<sup>5,6</sup> As the grating functions as a wavelength filter, only spontaneous emission wavelengths falling within the grating bandwidth will be reflected and amplified. Thus the grating determines a narrow bandwidth under which the laser may lase. In practice, grating lasers possess a linewidth much smaller than the grating linewidth ( $<100\text{pm}$  for a 10 mm long grating). For a nontunable grating laser, a linewidth of less than 100 MHz is possible which exceeds the standard ITU specifications.<sup>7</sup> In fact, linewidths as little as 103 kHz have been demonstrated in sampled fiber gratings.<sup>8</sup> In general, the cavity reflectivity and length will be the controlling factors in the design of a semiconductor laser. Higher rear facet and grating reflectivities along with longer cavities will narrow the laser linewidth. In addition to spectral linewidth, the side-mode suppression- ratio (SMSR) of secondary wavelength peaks is a very important performance factor. It is generally accepted that a 40 dB SMSR is required in telecommunication lasers. An estimate of the SMSR of the Telephotronics ECDL can be made with knowledge of the spectral width of the Bragg grating (FWHM, 0.1nm) and optical cavity length (15 mm, FP modes spaced at 0.07 nm intervals). By tuning the phase section of the waveguide so that one of the FP modes falls at the grating center, the filtering of the secondary side FP modes can be suppressed to less than 10% that of the center mode. The expected SMSR of a laser can be approximated by the relation:  $\text{SMSR} = (2 \cdot P \cdot \delta g) / (h \cdot \nu \cdot v_g \cdot n_{sp} \cdot \alpha_{tot} \cdot \alpha_m)$ , where P is the power of the light contained in the cavity [J/sec],  $\delta g$  is the differential gain of the main and secondary modes [0.6/cm],  $h \cdot \nu$  the energy of the 1.5  $\mu\text{m}$  photon,  $n_{sp} = 2$ ,  $\alpha_{tot}$  total cavity loss [4 /cm],  $\alpha_m$ , mirror loss [0.1/cm], and  $v_g$  is the speed of light in the (optical length )cavity ( $3 \cdot 10^{10}$  cm/sec).<sup>9</sup> The SMSR of the Telephotronics ECDL can be as high as 66 dB. The Telephotronics tunable ECDL has the required telecommunication characteristics of tunability over the entire Erbium C Band, narrow linewidth, large SMSR, and stability.

## 2.2. Thermo-Optic Tunable Filters

Tunable filters can be based on Bragg gratings, diffraction gratings, arrayed waveguide gratings (AWG's), microring resonators, or photonic crystals. In this section, we describe the characteristics of the thermally tunable Bragg gratings in polymeric waveguides, used in conjunction with laser chips (per the above-described design) to form tunable external cavity lasers.

The planar polymeric waveguides are designed to support a single spatial mode and to have a mode size comparable to that of the lasers. Gratings in polymer waveguides can be produced by a variety of techniques such as casting, molding, embossing, e-beam writing and photochemical processes.<sup>10,11</sup> The first three techniques produce surface relief gratings while the last two can produce either relief gratings or bulk index gratings across the waveguide core. Photochemical fabrication processes for bulk index gratings utilize two-beam interference to induce an index modulation. This effect can be achieved either through the use of a phase mask (where two beams corresponding to the +1<sup>st</sup> and -1<sup>st</sup> diffraction orders are allowed to interfere) or through the use of direct interference of split laser beams. For a waveguide refractive index of  $n = 1.5$ , the period of the grating corrugation, the Bragg period,  $\Lambda$ , is approximately 0.52  $\mu\text{m}$ . The magnitude and the filter width of the Bragg grating can be predicted using the following relations. Given a grating length of  $L = 10$  mm, an index modulation of  $\Delta n = 1 \cdot 10^{-4}$ , and a center design wavelength of  $\lambda_0 = 1.55$   $\mu\text{m}$ , the grating has a coupling constant  $\kappa = (\pi \cdot \Delta n) / (2 \cdot \lambda_0) = 1 \cdot 10^{-4}$  [ $\mu\text{m}^{-1}$ ]. At the Bragg wavelength, the power reflection coefficient is  $R = \tanh^2(\kappa \cdot L) = 0.58$ , and the bandwidth of the filter (FWHM) can be approximated by  $\Delta \lambda_{\text{FWHM}} = (\lambda_0 \cdot \Delta n) / (2 \cdot n) = 50$  pm.<sup>9</sup> The effective length of the grating is  $L_{\text{eff}} = \tanh(\kappa \cdot L) / (2 \cdot \kappa) = 2.9$  mm.

Tuning of the grating is achieved by powering a heater that is fabricated in the proximity of the grating. Broad thermal tuning of polymeric gratings is possible because of the large  $dn/dT$ . The value of  $dn/dT$  in the polymers used is  $-3.1 \times 10^{-4}/^\circ\text{C}$  (about 30 times larger than in glass), resulting in a channel tuning rate of  $-0.36$  nm/ $^\circ\text{C}$ . This figure translates into tuning across the entire Erbium C band (1528-1565 nm) with a temperature range of about 100 $^\circ\text{C}$ . Fig. 2 depicts the transmission spectra obtained when tuning the filter between 20 and 120 $^\circ\text{C}$ , demonstrating that a wavelength window of 37 nm can be covered with a single tunable filter.

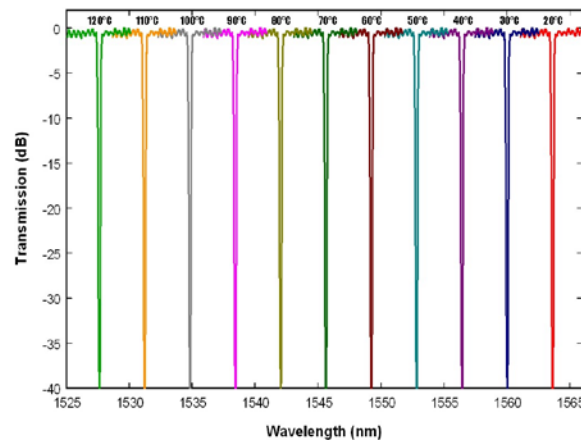


**Fig. 2.** Transmission spectra for a tunable filter operated between 20 and 120°C, covering the Erbium C band between 1528 and 1565 nm.

### 2.3. Integrated Magneto-Optic Isolators

In this section, the hybrid integration of isolators into polymeric optical circuits is described. All concepts for polarization independent isolators and circulators that have been proposed so far utilize interferometers. In one proposed implementation, such a polarization independent device consisted of a Mach-Zehnder interferometer with a half-wave retarder and a Faraday rotator in each arm, as shown in Fig. 3(a).<sup>12</sup> By having the two wave plates on opposite sides of the Faraday rotator and at an angle of 45° between their slow axes, constructive and destructive interference in forward and backward propagation direction is achieved, respectively. Another design that resembles the functionality of the micro-optical isolators and circulators is shown in Fig. 3(b). It consists of two integrated polarization splitters, a 45° Faraday rotator and a half-wave retarder. The first polarization splitter splits the TE and TM components of the incoming light into two separate arms. The light in each arm passes through the combination of Faraday rotator and half-wave plate where, depending on the propagation direction, the polarization remains unchanged or is rotated by 90°. The second polarization splitter then recombines the light from the two arms into one of the two output ports. The main advantage of this design over the previous one is that it can achieve much higher isolation ratios.

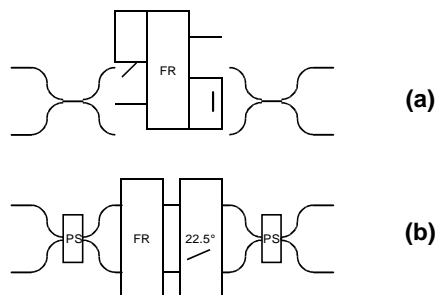


**Figure 3.** Circulator designs: The top design (a) consists of Mach-Zehnder interferometer with half wave retarders and Faraday rotator. The bottom design (b) consists of polarization splitters, Faraday rotator, and half wave retarder.

Even though considerable effort has been spent on the development of waveguide versions of various polarization optics elements, it has been shown in numerous reports that the hybrid integration of thin-film versions of those elements not only yields better performance but also has advantages in terms of fabrication. Thin-film polarizers and Faraday rotators that can be used for hybrid integration are technologically proven and in some cases are commercially available.

Thin-film polarizers called Lamipol, which consist of a stack of alternating silica and ultra-thin aluminum layers, are commercially available. They have a thickness (in the propagation direction) of 30µm, an insertion loss of <0.4 dB, and an extinction ratio of >55dB. Their high performance has been demonstrated in many different applications, including hybrid-integrated isolators.

Thin-film half-wave plates made of polyimide are also commercially available. They have a refractive index between 1.6 and 1.7, a thickness of  $\sim 16\mu\text{m}$ , an extinction ratio of  $>25\text{dB}$ , a Moh's hardness of 8 and negligible insertion losses. However, the material is hygroscopic and therefore requires a hermetically sealed package. So far, polyimide wave plates have been used to make hybrid integrated isolators and circulators as well as polarization independent Arrayed Waveguide Gratings (AWG). Another promising method to fabricate retarder plates is based on Crystal Ion Slicing (CIS) of birefringent single crystal such as lithium niobate. The CIS method is described in detail in the next section. An integrated polarization mode converter was demonstrated on a silica platform using a  $10.6\mu\text{m}$  thick lithium niobate CIS film as the half-wave plate. The device had an extinction ratio  $>30\text{dB}$  at  $1550\mu\text{m}$  wavelength.<sup>13</sup>

The most challenging task is the fabrication of thin-film Faraday rotators. The currently available  $45^\circ$  Faraday rotators have a thickness of typically about 0.5 mm and are therefore not suitable for the hybrid integration into planar lightwave circuits, simply because the diffraction loss that they would incur is too large. Also, since the Faraday rotator has a refractive index of about 2.2, a value that is significantly larger than that of silica or polymer, any tilting of the film would offset the beam path and cause large excess losses. Therefore, materials with higher specific Faraday rotation are needed in order to reduce the length of the rotator. Recently, several authors have grown epitaxial Cerium-substituted yttrium iron garnet films that have specific Faraday rotations of more than  $4500^\circ/\text{cm}$  at  $1.55\mu\text{m}$  wavelength, which corresponds to a length of less than  $100\mu\text{m}$  for  $45^\circ$  rotation. Although Ce:YIG has a fairly high absorption loss of about  $10\text{ dB/cm}$ , the total absorption loss of the Faraday rotator is only 0.1 dB. A larger problem is the diffraction losses, which are still in the order of 1 dB for a mode field diameter of  $10\mu\text{m}$ . One of the main advantages that polymer-based PLCs have over their silica counterparts is the greater flexibility of fabrication. Polymer waveguides can be made in many different ways such as direct photolithographic imaging, reactive ion etching, embossing, molding and casting. This flexibility makes it possible to fabricate a 3-dimensional taper that increases the mode size from  $10$  to  $20\mu\text{m}$  and thus reduces the diffraction losses to 0.3 dB.<sup>14,15</sup>

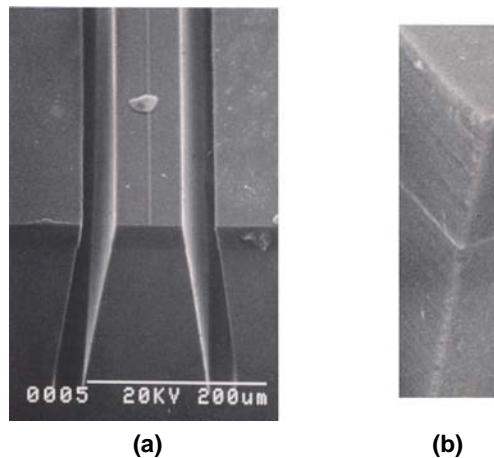


**Figure 4.** (a) Scanning electron micrograph of grooves fabricated by dicing (groove depth: 200mm, width: 40mm, tilt angle:  $8^\circ$ ), and (b) close up view of a diced facet.

The various thin-film components are integrated into the polymer platform by insertion into grooves. Such grooves with widths down to  $10\mu\text{m}$  can easily be fabricated in the polymer with a standard dicing saw. The process features excellent width control and yields remarkably smooth sidewalls with very few defects. Typical results are shown in Fig. 4. In order to measure insertion losses, liquid monomer was filled into the grooves and cured under UV light. The results are in good agreement with the calculated diffraction loss, which indicates that the scattering losses are negligible ( $<0.05\text{ dB}$ ).

Although many reports on magneto-optical devices do not mention the permanent magnet that is needed to uniformly magnetize the Faraday rotator, it has, in many cases, a considerable effect on the overall size of the device. Commercially available bulk Faraday rotators require  $\sim 100$  to  $1000\text{ Oe}$  to saturate the magnetization, however for waveguide rotators this value is typically one or two orders of magnitude lower. The required magnetic field depends on the crystal composition, the growth process and the geometry of the magneto-optic crystal. The smaller the ratio of the length to the

diameter of the Faraday rotator, the larger is the magnetic field that is needed to saturate it. Less than 2 kOe is required to saturate a few micrometer thick Ce:YIG film with a specific Faraday rotation of  $\sim 5000^\circ/\text{cm}$  along the film normal.<sup>16</sup> This makes the use of sputtered thin-film magnets practically impossible, since the magnets would have to be several hundred microns thick to generate such a strong field.

In our first experiments we used two neodymium iron boron magnets with dimensions of  $1 \times 3 \times 5 \text{ mm}^3$  and a remanent flux density of 10 kG parallel to the direction of beam propagation. They were placed on top of the polymer platform on both sides of the Faraday rotator as shown in Fig. 5.

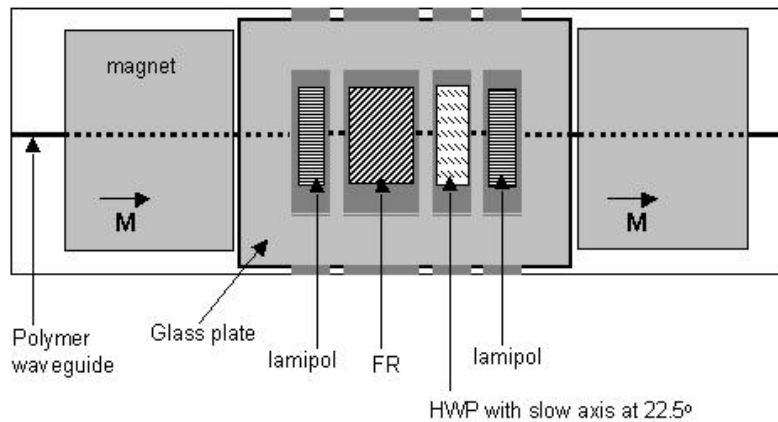


**Figure 5.** Fabricated hybrid integrated isolator based on Telephotronics OASIC™ platform.

We demonstrated the hybrid integration of nonreciprocal components into polymer-based PLCs by realizing an isolator within the Telephotronics Optical Application-Specific Integrated Circuit (OASIC™) platform.<sup>17</sup> In this experiment, a commercial Bi:YIG crystal with a thickness of  $450 \mu\text{m}$  was used as the  $45^\circ$  Faraday rotator. The field strength required to saturate the magnetization was about 500 Oe. In order to minimize the diffraction losses, waveguides with a mode diameter of  $20 \mu\text{m}$  were fabricated on a silicon substrate and grooves to accommodate the thin-film elements were diced perpendicularly to the waveguides. The groove for the Faraday rotator was  $460 \mu\text{m}$  wide, all other grooves were  $40 \mu\text{m}$  wide. All grooves were separated from each other by  $100 \mu\text{m}$ .

A thin lithium niobate film was used as the half-wave plate, as described above. Its slow axis was set at an angle of  $22.5^\circ$  relative to the Lamipol polarizers at the input and output of the device. Liquid monomer was poured into the grooves and solidified by UV curing in order to fix the components and minimize the scattering losses. Finally, two magnets were glued to the surface with a glass plate between them as a spacer. The observed magnetic field across the gap was 2 kOe, which was sufficient to saturate the Faraday rotator.

This device was fully packaged and optically measured at  $\lambda=1.55 \mu\text{m}$ . It exhibited an isolation of 15 dB and an excess loss of 2.2 dB. The excess loss is defined as the difference between the theoretically expected loss and the measured loss. It includes the fiber-connector losses, imperfect polarization rotation at the half-wave retarder and angular alignment errors of polarizing elements.

The diffraction losses of 2 dB can be significantly reduced when the  $450 \mu\text{m}$  thick Faraday rotator is replaced by multiple thin rotators. For instance, using 3 films of  $150 \mu\text{m}$  thickness reduces the diffraction loss by 1.2 dB, as can be seen in Fig. 6. Calculations show that with a Ce:YIG film as the Faraday rotator the overall insertion losses will be less than 1 dB.

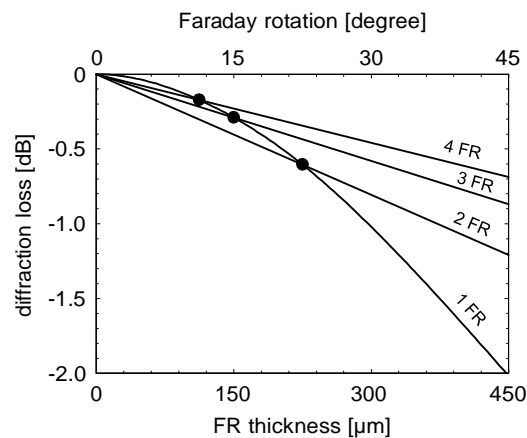


**Fig. 6.** The diffraction loss as a function of Faraday rotator thickness shows that the use of multiple thin rotators instead of a single thick rotator can significantly reduce the diffraction losses.

## 2.4. Low-Voltage Electro-Optic Modulators

The CIS process allows to produce thin crystal slices with optical properties identical to those of bulk crystals. We used this process to produce  $\text{LiNbO}_3$  thin films that can be used to form modulators with the lowest modulation voltage achieved in this material.

### 2.4.1. Crystal Ion Slicing and $\text{LiNbO}_3$ Films

The CIS process employs the formation and subsequent preferential etching of a buried damaged sacrificial layer obtained by implanting highly energetic ( $\sim\text{MeV}$ ) although light  $\text{He}^+$  particles into a single-crystal bulk material. As the

ions penetrate into the target they scatter and lose energy. At higher energies the scattering is primarily electronic with no lattice distortion, while at lower energies, the dominant stopping mechanism is governed by Rutherford scattering. The host nuclei thus become significantly dislodged towards the end of the ionic range, leading to the formation of a narrow damaged sacrificial layer well beneath the surface, which exhibits preferential etching upon immersion into an etchant solution. The energy of the implantation can be adjusted to select a desired film thickness, while the total dose ( $\sim 10^{16} \text{ cm}^{-2}$ ) will determine the amount of damage introduced in the sacrificial layer. Transport-of-ions-in-matter (TRIM) calculation is used to determine the ion range and implantation profile, and, thus, the thickness of the films to be obtained. For example, implanting at 3.8 MeV in  $\text{LiNbO}_3$  will result in  $\sim 10 \mu\text{m}$  thick films, while at 2.25 MeV the film thickness is  $\sim 5.2 \mu\text{m}$ .

#### 2.4.1.1. Wet-etch CIS lift-off

A deep undercut will form in the sacrificial layer during the etch process and uniformly progress with time, resulting in a freestanding CIS film.<sup>18,19</sup> In the case of  $\text{LiNbO}_3$ , the etchant normally used is diluted hydrofluoric acid. The etch selectivity, i.e. the ratio of the etch rates along and normal to the sacrificial layer plane, can be very high, and in the case of  $\text{LiNbO}_3$  are well above 1,000. By heat-treating the implanted bulk samples prior to etching, the etch rates and etch selectivity can be significantly enhanced by factors as large as 140.<sup>19</sup> We attribute this to the fact that upon implantation,  $\text{He}^+$  does not form a solid solution within the host matrix; heat treatment thus drives the ions to regions of large damage where they coalesce, generating additional vertical stress. This intuitive picture is corroborated by the Secondary Ion Mass Spectroscopy studies where the additional stress buildup due to  $\text{He}^+$  migration can be easily seen from the measured spectra. In addition, rapid thermal treatment was also found to be instrumental in removing the residual damage

in the film region after the implantation. X-ray diffraction measurements performed on  $\text{LiNbO}_3$  have shown that the detached films have the same crystallographic structure as virgin bulk, and little residual damage.<sup>18</sup> However, full removal of the residual mechanical stress and the implantation-related alterations of the material properties (e.g. slight departures of the measured refractive indices from the bulk values) can be fully removed only by annealing the fabricated films in a flowing oxygen atmosphere at high temperatures. Conversely, ion implantation induced shifts in refractive indices can be utilized to tailor the optical properties of thin films, such as the phase-matching condition for efficient guided-wave nonlinear optical interactions.<sup>20</sup>

### 2.4.1.2. Thermal shock CIS lift-off

An alternate route to fabricating thin CIS films has also been implemented.<sup>21,22</sup> Thermal shock, in a form of a rapid temperature increase is applied to the implanted material, resulting in the lateral pressure release in the sacrificial (implanted) layer, and a subsequent separation of the CIS film from its parent wafer. The underlying physical mechanism for thermal lift-off is in fact similar to the wet-etch process described above. The films obtained by this process are of comparable quality.

### 2.4.1.3. CIS film morphology

Although films as large as  $\sim 15 \times 15$  mm were obtained, the CIS technique is particularly useful for fabrication of longer ( $>20$  mm) and narrower ( $\sim 3$  mm) slices, as it is the shorter film dimension that determines the time required for (wet-etch) lift-off. These dimensions are in accord with wafer sizes normally used for fabrication of conventional  $\text{LiNbO}_3$

optical circuits. The fabricated CIS films are typically  $4\text{--}10\ \mu\text{m}$  thick (for energies  $1.8\text{--}3.8$  MeV, respectively) while the general fabrication process appears to be independent of the crystallographic orientation.<sup>19</sup> The CIS process is also found transparent to the direction of the spontaneous material polarization; thus, an arbitrary polarization domain structure can be preserved upon ion implantation, subsequent heat treatment and wet etching.<sup>23</sup> This fact was effectively used to produce thin films of periodically poled  $\text{LiNbO}_3$  material for quasi phase-matched frequency conversion with bulk-like response at  $1550$  nm, as well as for fabrication low-noise bicell CIS film pyroelectric detectors for acoustic nulling.<sup>23,24</sup>

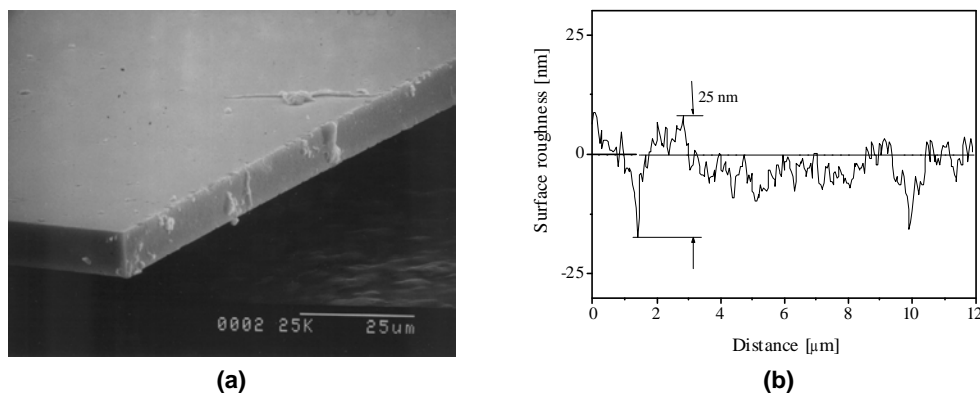


**Fig. 7.** Flatness of a  $10\text{-}\mu\text{m}$ -thick Z-cut CIS  $\text{LiNbO}_3$  slab as seen under a scanning electron micrograph (a) and under an atomic force microscope (b). The roughness is  $5$  nm *rms* and the roughness range is approximately  $25$  nm over the scanned area.

Figure 7(a) features a scanning electron micrograph of a CIS film of  $\text{LiNbO}_3$  placed on a glass platform. As can be inferred from the figure, the CIS process does not degrade the facet film quality (polished prior to liftoff). In the case of wet-etch CIS liftoff, the top film surface can generally be affected by the etchant, but this effect can be readily suppressed by applying an appropriate protective layer. This is particularly important in fabricating pre-patterned active optical circuits in thin CIS films.<sup>25</sup> The underside film surface corresponding to the sacrificial layer is somewhat rougher; however, it is still quite smooth relative to the wavelengths of interest ( $\sim 1550$  nm), with a typical *rms* roughness value of

$<10$  nm (the *rms* for the AFM scan shown in Fig. 7(b) is  $5$  nm). Thus, the morphology of the CIS  $\text{LiNbO}_3$  films is essentially compatible with the integrated optics devices needs.

Different methods have been studied in order to integrate CIS films with important heterogeneous substrates, such as InP, Si and GaAs. Once fabricated, the thin films can easily be mounted on an arbitrary planar surface and held firm via the attractive Van der Waals force. Bonding can also be achieved by applying an etchant-proof epoxy, wax, or polymer between the top film surface and the hetero-substrate prior to lift-off. Direct low-temperature ( $200^\circ\text{C}$ ) pre-liftoff bonding between  $\text{LiNbO}_3$  and InP, and  $\text{LiNbO}_3$  and Si was realized, using a procedure similar to that described elsewhere in the literature.<sup>26</sup> Other methods such as anodic bonding, wafer bonding, metal or polymer bonding can also be applied in the hetero-integration process.

Crystal ion sliced LiNbO<sub>3</sub> films have been used in both normal-incidence and in-plane light propagation device applications. The former include compact polarization-control building blocks for integrated optics circuits,<sup>22,27</sup> as well as low-noise pyroelectric optical detectors.<sup>28</sup> The latter are related to conventional LiNbO<sub>3</sub> devices transferred onto thin CIS films, namely passive optical circuits with annealed proton exchanged waveguides,<sup>25</sup> and also as active circuits in the form of thin-film optical modulators.<sup>29,30</sup>

#### 2.4.2. Low-Voltage CIS-Based Electro-Optic Modulators

CIS films have the advantage of being only a few microns thick, thus allowing for low-voltage applications via the largest electro-optical coefficients in devices where such a control is desired. More importantly, they are particularly attractive for offering novel approaches to designing low-voltage impedance- and velocity-matched modulators, obviating the need for buffered oxide layers, and therefore eliminating the microwave losses associated with this layer, while at the same time increasing the overlap between the optical and the microwave field, and, therefore, lowering the  $V_{\pi}L$  product.<sup>30</sup>

$\chi^{(2)}$ -related optical properties of the CIS LiNbO<sub>3</sub> material have been measured, and found to be equal to, or closely approximate to the bulk values.<sup>20,29</sup> Electro-optical coefficients ( $r_{33}$ ,  $r_{13}$ ) were determined using an intensity modulator configuration (input light at 45° relative to the TE/TM polarization). The film was sandwiched between two metal electrodes; no buffer oxide layer was employed in this experiment. The measured  $V_{\pi}L$  product required for optical switching at 1550 nm was ~8 Vcm,<sup>29</sup> while a theoretical value of  $V_{\pi}L = \lambda \cdot d / |n_e^3 \cdot r_{33} - n_o^3 \cdot r_{13}| \approx 7.4$  V·cm is obtained for an ideal thin-film intensity modulator with bulk properties. Given that the measured CIS film birefringence closely approximates bulk values, the electro-optical coefficients of the thin CIS material are essentially those of the single-crystal bulk.

A practical thin CIS film modulator has not yet been reported. However, theoretical studies have shown possibilities for significant improvements using a thin, 5–10- $\mu$ m-thick CIS film design without the use of buffer oxide layers. Further, by appropriately designing a modulator in which the thin CIS film is residing on a low dielectric constant material, a greater portion of the microwave field can be forced to propagate in the film substrate, reducing the overall effective index and facilitating velocity matching.

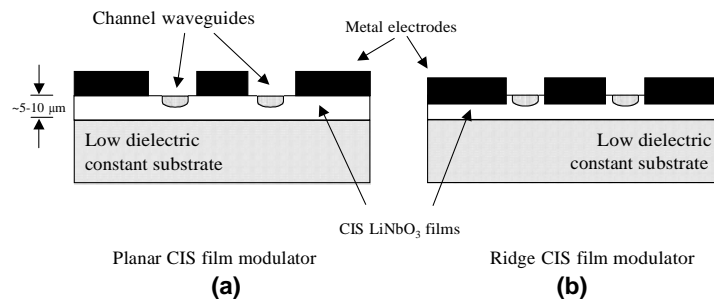


**Fig. 8.** Two Mach-Zehnder type CIS film modulator designs for optimized modulator performance. The thick conventional approach requires the use of a buffer oxide layer to compensate for velocity mismatch resulting in increased microwave losses and higher drive voltages.

Several different Mach-Zehnder-type waveguide thin-film modulator configurations in X-cut CIS LiNbO<sub>3</sub> with coplanar electrodes and no oxide layer were considered (Figure 8).<sup>30</sup> Table 1 compares the important modulator parameters of the thin-film modulator without ridges (Fig 8(a)) with the bulk modulator design having a buffer oxide layer.<sup>31</sup> The thin-film modulator parameters are 25  $\mu$ m for the electrode gap, 5 $\mu$ m / 16 $\mu$ m for the electrode width/thickness, 6  $\mu$ m for the CIS film thickness, and 4 for the substrate relative dielectric constant. The results from Table 1 suggest that the CIS film design will have the same modulation bandwidth and a somewhat improved impedance matching. However, due to the absence of the buffered oxide layer and increased overlap between the optical and the microwave fields, the  $V_{\pi}L$  product is reduced by about 20%. For example, a modulator with a 16-mm-long electro-optically active region that would have a  $V_{\pi}$  of 5.9 V in bulk LiNbO<sub>3</sub>, exhibits a  $V_{\pi}$  of 4.8 V when implemented with the CIS technology.

**Table 1.** Comparison between an oxide-free, thin-film CIS modulator on X-cut LiNbO<sub>3</sub> and an equivalent bulk design with a buffer layer (no ridges present)

	CIS film modulator without buffer oxide <sup>30</sup>	Thick Z-cut modulator with buffer oxide <sup>31</sup>
Microwave losses, $\alpha$ , [dB/(cm·GHz <sup>0.5</sup> )]	~0.33	~0.33
Characteristic impedance, $Z_c$ [ $\Omega$ ]	48	43
Velocity-matching	Yes	Yes
Voltage – length product, $V_{\pi}L$ [V·cm]	~7.7	~9.4

A comparison of results for a ridge film modulator (Fig. 8(b)) with the bulk version of similar design parameters<sup>32</sup> also shows improvement in the thin-film approach. While the bulk design<sup>32</sup> suffers from significant velocity mismatch, the CIS ridge film modulator with a width/thickness of 8 $\mu$ m/22 $\mu$ m, an electrode gap of 25 $\mu$ m, base film thickness of 3  $\mu$ m and a ridge height of 2  $\mu$ m, is matched. Further, the CIS design exhibits low microwave losses (0.3 dB/cm·GHz<sup>0.5</sup>), impedance matching (~49  $\Omega$ ), and a low  $V_{\pi}L$  product of ~7.0 V·cm. By extending the electrode gap, the CIS film microwave attenuation can be additionally minimized (to as low as 0.26 dB/cm·GHz<sup>0.5</sup>), however, at the expense of a somewhat increased  $V_{\pi}L$  product.

### 2.5. Integrated Tunable Optical Transmitters

The different polymer-optical-bench-based integrated optic technologies described above are compatible with one another, and they can be combined on a single chip to form an integrated transmitter that comprises a tunable laser, an isolator, and a modulator (Fig. 9). This is the first complete optical transmitter to be integrated on a single chip.

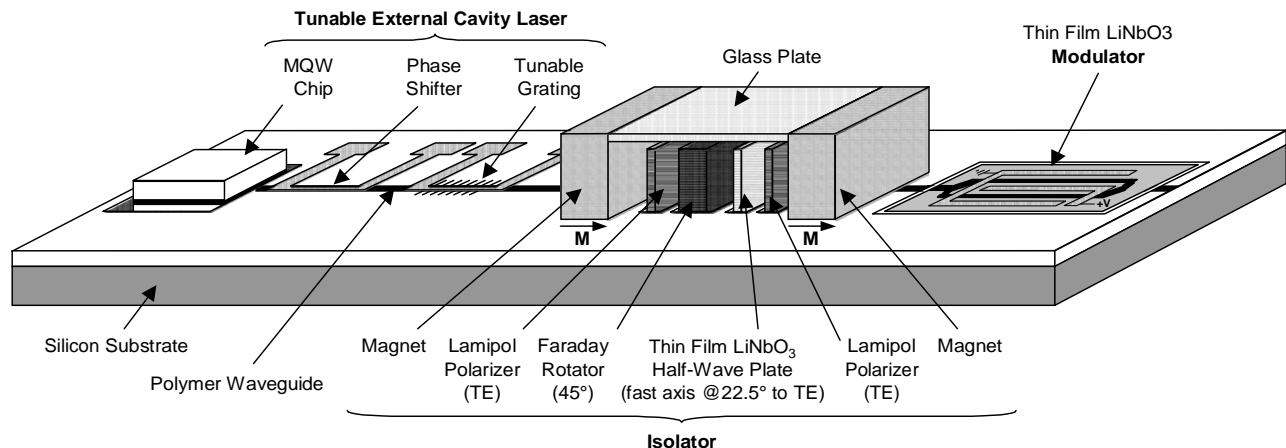


**Fig. 9.** Optical transmitter comprising a tunable laser, an isolator, and a modulator, integrated on a single silicon chip using a polymer optical bench platform.

## 3. CONCLUSION

We described different polymer-optical-bench-based integrated optic technologies, including tunable Bragg-grating-based filters, tunable external cavity lasers, isolators, and low-voltage modulators. These technologies were combined on a single chip to form the first fully integrated transmitter. This single-chip transmitter exhibits most advantages of integration including size reduction, performance improvement, automated fabrication and assembly, increase in yields, increase in production volumes, reduced cost, and faster time to market.

## REFERENCES

1. M. Tohyama, M. Onomura, M. Funemizu, and N. Suzuki, "Wavelength tuning mechanism in three-electrode DFB lasers," *IEEE Photon. Technol. Lett.* **5**, 616 (1993).
2. K. Kobayashi and I. Mito, "Single frequency and tunable laser diodes," *J. Lightwave Technol.* **6**, 1623 (1988).
3. F. Delorme, *IEEE J. Quant. Electron.* **34**, 1706 (1998).
4. P.-J. Rigole, S. Nilsson, L. Backbom, T. Klinga, J. Wallin, B. Stalnacke, E. Berglind, B. Stoltz, "Access to 20 evenly distributed wavelengths over 100 nm using only a single current tuning in a four-electrode monolithic semiconductor laser," *IEEE Photon. Technol. Lett.* **7**, 1249 (1995).
5. T. Day, M. Brownell, and I.-F. Wu, "Widely tunable external cavity diode lasers," *SPIE* **2378**, 35 (1995).
6. P. Zorabedian and W. R. Trutna, Jr., "Interference-filter-tuned, alignment-stabilized, semiconductor external-cavity laser," *Optics Lett.* **13**, 826 (1988).
7. Y. Akahori, T. Ohyama, M. Yanagisawa, Y. Yamada, H. Tsunetsugu, Y. Akatsu, M. Togashi, S. Mino, and Y. Shibata, "Integrated external cavity laser composed of spot-size converted LD and UV written grating in silica waveguide on Si," *Electron. Lett.* **32**, 1202 (1996).
8. J.-F. Lemieux, A. Bellemare, C. Latrasse, and M. Tetu, "Step-tunable (100GHz) hybrid laser based on Vernier effect between Fabry-Perot cavity and sampled fibre Bragg grating," *Electron. Lett.* **35**, 904 (1999).
9. M. Amann and J. Buus, *Tunable Diode Lasers*, Artech House (1998).
10. L. Eldada and L.W. Shacklette, "Advances in polymer integrated optics," *IEEE J. Select. Top. Quant. Electron.* **6**, 54 (2000).
11. L. Eldada, "Polymer-based filters for DWDM applications," *OSA TOPS WDM Components* **29**, 105 (1999).
12. N. Sugimoto, T. Shintaku, A. Tate, H. Terui, M. Shimokozono, E. Kubota, M. Ishii, and Y. Inoue, "Waveguide polarization-independent optical circulator," *IEEE Photon. Technol. Lett.* **11**, 355 (1999).
13. A. M. Radojevic, R. M. Osgood, Jr., M. Levy, A. Kumar, and H. Bakhru, "Zeroth-order half-wave plates of LiNbO<sub>3</sub> for integrated optics applications at 1.55 $\mu$ m," *IEEE Photon. Technol. Lett.* **12**, 1653 (2000).
14. L. Eldada, "Polymeric Optoelectronic Interconnects," Photonics West conference, *Proc. SPIE* **3952A**, 190 (2000).
15. R. Inaba, M. Kato, and H. Akahoshi, "Improved coupling efficiency using  $\Delta n$ -controlled polymer waveguides with two-dimensional spot-size transformation," *IEEE Photon. Technol. Lett.* **12**, 404 (2000).
16. M. Gomi, S. Satoh, and M. Abe, "Giant Faraday rotation of Ce-substituted YIG films epitaxially grown by RF sputtering," *Jpn. J. Appl. Phys.* **27**, L1536 (1988).
17. J. Fujita, R. Gerhardt, and L. Eldada, "Hybrid Integrated Optical Isolators and Circulators," Photonics West conference, *Proc. SPIE* **4652A** (2002).
18. M. Levy, R. M. Osgood Jr., A. Kumar, and H. Bakhru, "Crystal ion-slicing of magnetic and ferroelectric oxide films," *App. Phys. Lett.* **71**, 2617 (1997).
19. A. M. Radojevic, M. Levy, R. M. Osgood Jr., A. Kumar, H. Bakhru, C. Tian, C., and C. Evans, "Large etch selectivity enhancement in the epitaxial liftoff of single-crystal LiNbO<sub>3</sub> films," *Appl. Phys. Lett.* **74**, 3197 (1999).
20. A. M. Radojevic, M. Levy, M. H. Kwak, and R. M. Osgood, Jr., "Strong nonlinear optical response in epitaxial liftoff single-crystal LiNbO<sub>3</sub> films," *App. Phys. Lett.* **75**, 2888 (1999).
21. J. H. Lehman, A.M. Radojevic, R.M. Osgood, Jr., and M. Levy, "Fabrication and evaluation of a freestanding pyroelectric detector made from single-crystal LiNbO<sub>3</sub> film," *Optics Lett.* **25**, 1657 (2000).
22. A. M. Radojevic, M. Levy, R. M. Osgood, Jr., A. Kumar, and H. Bakhru, "Zeroth-order half-wave plates of LiNbO<sub>3</sub> for integrated optics applications at 1.55  $\mu$ m," *IEEE Photon. Technol. Lett.* **12**, 1653 (2000).
23. A. M. Radojevic, M. Levy, R. M. Osgood, Jr., D. H. Jundt, A. Kumar, and H. Bakhru, "Second-order optical nonlinearity of 10- $\mu$ m-thick periodically poled LiNbO<sub>3</sub> films," *Optics Lett.* **25**, 1034 (2000).
24. J. H. Lehman, A. M. Radojevic, and R. M. Osgood, Jr., "Domain-engineered thin-film LiNbO<sub>3</sub> pyroelectric-bicell optical detector," *IEEE Photon. Technol. Lett.* **13**, 851 (2001).
25. A. M. Radojevic, R. M. Osgood, N. A. Roy, and H. Bakhru, "Pre-patterned optical circuits in thin ion-sliced single crystal films of LiNbO<sub>3</sub>," *IEEE Photon. Technol. Lett.* **14** (2002).
26. T. Izuhara, M. Levy, and R. M. Osgood, Jr., "Direct wafer bonding and transfer of 10- $\mu$ m-thick magnetic garnet films onto semiconductor surfaces," *Appl. Phys. Lett.* **76**, 1261 (2000).
27. A. M. Radojevic, M. Levy, R. M. Osgood, Jr., and H. Bakhru, "Zero-order half-wave plates of lithium niobate for integrated optics applications in the 1.55- $\mu$ m waveband," *Trends in Optics and Photonics, Int. Photon. Res.* **45**, 271 (2000).
28. J. H. Lehman, and J.A. Aust, "Bicell pyroelectric optical detector made from a single LiNbO<sub>3</sub> domain-reversed electret," *Appl. Opt.* **37**, 4210 (1998).
29. T. Ramadan, M. Levy, and R. M. Osgood, Jr., "Electro-optic modulation in crystal-ion-sliced z-cut LiNbO<sub>3</sub> thin films," *Appl. Phys. Lett.* **76**, 1407 (2000).
30. I-L. Gheomra, P. Savi, and R. M. Osgood, "Thin layer design of X-cut LiNbO<sub>3</sub> modulators," *IEEE Photon. Technol. Lett.* **12**, 1618 (2000).
31. W. K. Burns, M. M. Howerton, R. P. Moeller, R. Krähenbühl, R. W. McElhanon, and A. S. Greenblatt, "Low drive voltage, broad-band LiNbO<sub>3</sub> modulators with and without etched ridges," *J. Lightwave Technol.* **17**, 2551 (1999).
32. S.-J. Chang, C.-L. Tsai, Y.-B. Lin, J.-F. Liu, and W.-S. Wang, "Improved electrooptic modulator with ridge structure in X-cut LiNbO<sub>3</sub>," *J. Lightwave Technol.* **17**, 843 (1999).

**For more information  
visit [www.enablence.com](http://www.enablence.com)**